—DRAFT—

SNO-STR-97-009

High Energy Gamma-Rays measurements in the SNO Cavity

M.C. Perillo Isaac, Y.D.Chan, D.L. Hurley, K.T. Lesko, M.E. Moorhead, E.B. Norman, A.R. Smith
Lawrence Berkeley National Laboratory

D.L. Cluff, D. Hallman
Laurentian University

J. Heise
University of British Columbia

P. Jagam
University of Guelph

Abstract

We report the results of a series of measurements of the gamma-ray flux in the Sudbury Neutrino Observatory (SNO) cavity after its completion. The measurements were done with a large volume NaI detector for 62 days on the floor of the SNO cavity. The response of the SNO detector to high energy, above 3-4 MeV, gamma-rays is studied.

Contents

1 Introduction 4

2 Measurements and Data Analysis 5

2.1 The NaI Efficiency an Response 5

2.2 The measured flux of 1460 and 2614 keV 6

2.3 The measured gamma flux above 3 MeV 8

2.4 The effect in SNO of gamma flux above 3 MeV 10

3 Comments and conclusions 12

4 References 12

List of Figures

1 Figure 1: Absolute NaI Efficiency 14

2 NaI Response 14

3 Ge spectrum 15

4 NaI spectrum 16

5 Data at 6800 and 4600 ft 17

6 Spectra solution 17

7 Preogetion of GEANT generation 18

8 Water Geometry 19

9 Air Geometry 19

10 SNO response - water 20

1 Introduction

The Sudbury Neutrino Observatory (SNO) is a water Cerenkov detector built to measure the spectrum and the flux of neutrinos coming from our Sun. SNO is located 6800 ft below the surface (7000 meters water equivalent) in the Creighton mine in Sudbury, Ontario, Canada [1].

The SNO detector is sensitive high energy neutrinos from the the decay of ^{8}B in the Sun and from the ^{3}He + p fusion reaction. The ν_e's are detected mainly through the charged current reaction, equation (1). The unique characteristics of the SNO detector is its D_2O target which allows for the detection of any type of neutrinos ν_x, through the neutral current reaction, described in equation (2). Elastic scattering, equation (3), also occurs in the detector although its cross section is around a factor of 10 smaller than the cross sections for reactions (1) and (2). The expected counting rates for the charged current and the neutral current reactions are of the order of 10 events per day, according to the electron-neutrino flux predicted by the Standard Solar Model [2]. The expected counting rate of elastic scattering events is of the order of 1 event a day.

$$\nu_e + d \longrightarrow p + p + e \tag{1}$$

$$\nu_x + d \longrightarrow \nu_x + p + n \tag{2}$$

$$\nu_x + e \longrightarrow \nu_x + e \tag{3}$$

Backgrounds are clearly a determining factor for the success of any experiment which, like SNO, is faced with counting rates as low as a few events per day. The signal is obtained by the detection of either an electron (charged current reaction and elastic scattering) or by the detection of a neutron (neutral current reaction). High energy gamma rays are an important background for both charged and neutral current reactions since it can mimic exactly the signal we expect and do not allow for any discrimination. Compton scattering and/or pair production of high energy gamma-rays mimic the electron produced in the charged current reaction. The photodisintegration of the deuteron can produce neutrons which can be regarded as the neutral current reaction signal.

Gamma-rays with energies up to 10 MeV can be produced by natural radioactivity. Most of the naturally occurring radioactive isotopes decay by alpha emission. Since these radioactive isotopes are imbedded in the rock and other materials, the alpha particles can induce gamma-rays by (α, γ), $(\alpha$,n $\gamma)$ and $(\alpha$,p$\gamma)$ reactions on light nuclei [3,4]. Our goal with this work is to understand and evaluate the implications for the SNO detector of high energy gamma rays produced by these reactions in the rock. The results presented in this work are based on recent measurements of the gamma-ray flux in the SNO cavity performed with a large volume NaI detector. In the following sections we describe the experimental methods, analysis and results of this measurement. We also evaluate the consequences of the high energy gamma-ray flux as measured for the SNO experiment.

2 Measurements and Data Analysis

We used a 19 cm diameter by 15 cm thick NaI crystal to which three photomultiplier tubes (PMT) were attached. The gains of the PMT were matched and the signals all of the PMT's were summed and fed into a ORTEC-NOMAD, a portable data acquisition system.

The data is summarized in table 1. Nine runs were obtained with the NaI detector unshielded at the bottom of the SNO cavity. Other data were obtained at the 4600 ft level in different conditions: unshielded, shielded by 2 inches of copper plus 8 inches of lead and with a lead-only shield 8 inches thick. We also included in the overall analysis a spectrum acquired with a high purity Germanium detector when the cavity was only bare rock.

Table 1: Summary of data used in this work.

Spectrum	Time (hours)	Experimental Condition
SNOA to SNOI	1490	Unshielded at bottom of cavity - NaI
SNPA	429	4600 ft with 2" Cu + 8" Pb
SNPB	247	4600 ft with 8" Pb
SNPC	188	4600 ft unshielded
SNOGE	21	Unshielded bottom of unfinished cavity - Ge

2.1 The NaI Efficiency an Response

In order to evaluate the measured gamma-ray flux, one needs to know the intrinsic detection efficiency of the detector used. Equation (4) shows the relationship between the intrinsic efficiency ϵ_I and the absolute efficiency ϵ_A:

$$\epsilon_I = \epsilon_A \frac{4\pi}{\Omega} \tag{4}$$

where Ω is the solid angle in steradians subtended by the detector at the source position. The intrinsic detection efficiency was obtained by measurements of the absolute detection efficiencies and evaluating the solid angle Ω. Point calibration sources were positioned at different distances facing different surfaces of the detector in order to obtain an average intrinsic efficiency for the detector as a whole. We used point sources of ^{137}Cs , ^{60}Co and ^{228}Th at two different distances facing the bottom, the top (where the PMT's are mounted) and the cylindrical surfaces of the detector. The radioactive sources provide calibration points below 3 MeV. The evaluation of the efficiency above this energy was calculated by Monte Carlo.

Figure 1 shows the absolute photopeak detection efficiency of the detector as measured at 19 inches with the source facing the bottom of the detector. Results from Monte Carlo calculations performed using GEANT 3.21 [5] are also shown. In this figure, Monte Carlo values are systematically above the experimental points because the simulation takes into account only energy deposition, i.e., it does not treat details of the light collection. A correction factor of 0.8 was applied to the efficiency obtained by Monte Carlo in order to account for this effect. Note the good agreement between the experimental

data and the simulated data after this correction is applied. It is worth noting that escape peaks also contribute to the quoted photopeak efficiency because of the energy resolution of the apparatus at higher energies. The experimental energy resolution was included in the simulated data. Figure 2 presents the qualitative comparison between Monte Carlo and data from the NaI crystal for the ^{228}Th source as an example of the response of the detector to external gamma rays.

2.2 The measured flux of 1460 and 2614 keV

We studied the fluxes of the two most intense gamma-rays in the natural radioactive background: the 1460 keV line from the decay of ^{40}K and 2614 keV line from the decay of ^{208}Tl . The results were then compared to previous measurements made before the cavity was covered with shotcrete.

When the cavity was only bare rock, a 20-hour background measurement was performed with a HPGe detector. The HPGe crystal has a diameter of 7.4 cm and is 9.32 cm long. Its energy resolution is 1.8 keV at 1.33 Mev. Although the the low efficiency of HPGe at high energies does not allow for any estimate of the gamma flux above 3 MeV, the spectrum is well defined below this energy, as shown in figure 3. After the cavity was completed, a large volume NaI detector accumulated data for 1490.41 hours in May/96. The spectrum corresponding to this more recent measurement is shown in figure 4.

From the data in figures 3 and 4 and the experimental values for the detection efficiencies from both HPGe and NaI detectors, we obtained the flux of 1460 keV and 2614 keV gamma lines before and after the cavity was completed. The results are summarized on table 2. Both detectors' intrinsic backgrounds are negligible compared to the total counting rate. It amounts, in the case of the NaI, to at most 1% for the 1460 keV line and 0.5 % for 2614 keV line.

Table 2: Measured Fluxes - 6800 ft Level.

E_γ (keV)	Flux 3/94 $cm^{-2}s^{-1}$	Flux 5/96 $cm^{-2}s^{-1}$
1460	0.059 ± 0.003	0.0604 ± 0.006
2614	0.016 ± 0.001	0.00746 ± 0.0007

Previous measurements of U and Th contamination in the rock, shotcrete and urylon were used to relate the gamma flux to the natural radioactive contamination in these materials. The radioactive contamination contents in U, Th and K and in the norite was obtained by A. Smith [6] by direct gamma counting. Samples from various depths were collected during the excavation from October/91 to May/93. The radioactive contamination contents in shotcrete was measured in by M. Chen and is reported in [7]. Shotcrete samples from the SNO cavity lining were collected at various heights and the radioactive contamination was also measured by direct gamma counting. Urylon was measured at the Ultra Low Background detector at Guelph in 1992 [8]. The results of these measurements are summarized in table 3. Note that only limits for Urylon contamination in Th and U could be accessed.

Table 3: Contamination in Norite, Shotcrete and Urylon.

Material	U (ppm)	Th (ppm)	K (%)
Norite	1.10 ± 0.09	5.10 ± 0.48	1.032 ± 0.094
Shotcrete	1.188 ± 0.034	2.392 ± 0.134	0.7519 ± 0.0509
Urylon	< 0.003	< 0.009	0.85 (1)

According to these measurements, norite and shotcrete have approximately the same contamination contents of U; norite has about 2 times more Th than shotcrete and norite has about 30% more K than shotcrete and the contamination in Urylon in U and Th is quoted as an upper limit.

We studied a simple one dimensional model to evaluate the flux of gamma-rays exiting a 3 layer wall. We considered an infinitely thick norite layer, a 20 cm thick shotcrete layer and a 2 cm thick Urylon layer with the U and Th concentrations quoted in table 4. Urylon is responsible for 4.4% of the flux of 1460 keV gamma-rays while shotcrete contributes with 95.05% and the norite contributes with 0.05%. In the case of the flux of 2614 keV gammas in the cavity the contribution of the Urylon contamination is 0.095%; shotcrete is responsible for 93.97%, and norite contributes with 6.53% to the total flux. Hence, according to this model, the contamination in shotcrete is responsible for the bulk of the observed flux of gamma-rays in the cavity, suggesting that the measured flux should scale with the shotcrete contamination. The actual thickness of the shotcrete layer remains unknown.

Measurements of the gamma flux in the cavity do not show variation in the flux of 1460 keV gammas while the flux of 2614 keV gammas decreased a factor of 2 after the lining of the cavity with shotcrete.

The measured flux of the 2614 keV gamma-ray confirms the model. On the other hand the flux of 1460 keV as measured in 1996 is the same as the flux measured in 1992. According to the model described above, it should be 30% smaller, scaling with the ^{40}K contamination in shotcrete. Systematic errors in the flux measurement cannot account for this discrepancy. The major source of systematic errors in our flux evaluation comes from the efficiency determination: 10%. The systematic errors were estimated with various measurements of point calibration sources at various distances from the detector.

Another possibility is that, due to the coating of the cavity with urylon, the radon emanations from the rock decrease. The flux of the 609 keV gamma-ray line from ^{207}Bi (^{238}U chain) would provide another handle to this problem. Unfortunately the lower level discriminator in the NaI measurements is set to high to allow for a meaningful value for its flux.

Measurements of natural radioactive contamination by direct gamma counting can present systematic errors of the order of 30% or higher, depending on the samples and efficiency determinations. Also, systematic uncertainties related the evaluation of the contamination in ^{40}K are fundamentally different than those related to ^{232}Th contamination. Other factors can also contribute to the discrepancy we observe, such as ^{40}K hot spots around the site where the detector was taking data.

In order to check the consistency of our methods, we compared data obtained with our NaI detector at the low background facility at the 4600 ft level of Creighton mine with previous data from the same

location obtained by J.J. Thiessen [9] in 1992. We used his data to compare the fluxes of 1460 and 2614 keV in the lab at the 4600 ft level in 1992 and now. The results are presented in table 4. We observe a very good agreement between these measurements, ensuring that our detector is still working properly after being transported from 6800 ft level to 4600 ft level, and that our methods are consistent.

Table 4: Measured Fluxes - 4600 ft Level.

E_γ (keV)	Flux 1992 $cm^{-2}s^{-1}$	Flux 1996 $cm^{-2}s^{-1}$
1460	0.128	0.127 ± 0.028
2614	0.026	0.027 ± 0.005

2.3 The measured gamma flux above 3 MeV

The first step to understand the gamma-ray flux inside the cavity at high energies is to understand the detector's own background. This is particularly important if we are interested in an energy range where internal alpha and beta contamination, present at very low levels in the crystal, amount to a significant fraction of the total counting rate.

Measurements were performed in the low background facility at the 4600 ft level, where the availability of shielding and depth allow for data free of cosmic rays and environmental radioactivity. Two measurements were performed with different shielding: a composed shielding of Cu and Pb attenuates a fraction of the environmental neutrons as well as the gamma-rays; and a heavy lead only shielding. Figure 5 presents a comparison of the data obtained at:

a) 6800 ft level unshielded,
b) 4600 ft level unshielded,
c) 4600 ft level shielded with only 8 inches of Pb,
d) 4600 ft level shielded with 2 inches of Cu and 8 inches of Pb.

The spectra in figure 5 were compressed in 50 keV per bin and normalized to counts per hour per bin. It is clear that the backgrounds at the 4600 ft level are more intense than in the SNO cavity. The spectra obtained with the different shielding, i.e., lead only and with a lead/copper shield in the 4600 ft are also distinct since another background component, due to thermal neutron capture in the NaI crystal, is also present.

It is possible to use the data with different shielding to infer the flux of high energy gamma-rays above 3 MeV. The spectra *a)*, *b)*, *c)* and *d)* can be broken down into their components:

$$\begin{cases} a = & I + n_1 + \gamma_1 \\ b = & I + n_2 + \gamma_2 \\ c = & I + n_2 \\ d = & I + \alpha \times n_2 \end{cases} \tag{5}$$

where I represents the internal background of the detector due to contamination of the crystal in Th and U daughters; $n_{1(2)}$ represents the contribution to the spectrum due to the ambient neutron flux in

the SNO cavity (laboratory at 4600 ft level) and $\gamma_{1(2)}$ is the contribution due to ambient gammas at the SNO cavity (laboratory at 4600 ft level). The factor α comes from the attenuation of neutrons by 2 inches of copper in the shielding. The numerical value of α was evaluated using randomly generated particle's trajectories in the copper shielding and the mean free path of thermal neutrons in copper.

We can solve this system of equations for γ_1 if we assume that the neutron fluxes n_1 and n_2 are proportional to the measured flux of 2614 keV gamma-rays, i.,e., the Th contents. For the purpose of our evaluation, the assumption that that the neutron flux will scale with the thorium contamination in the rock is arbitrary, although reasonable and based on our experimental measurements. The actual neutron flux in the cavity remains unknown since it was not possible to perform different shielded measurements on site.

We were able to estimate the neutron flux at the 4600 ft level, using the data from spectra *c)* and *d)*, and obtaining the neutron induced spectrum in the NaI detector. Based on the excess of 5.65 ± 0.13 counts/hour above 4 MeV in the spectrum n_2 and on the neutron capture probability in the lead shielding and in the volume of the detector, we estimate the neutron flux in the 4600 ft laboratory to be of the order of 2.7×10^{-6} neutrons/cm^2/s. We quote for comparison the the thermal neutron flux measured with BF_3 counters at the Gran Sasso underground laboratory: $1.98 \pm 0.05 \times 10^{-6}$ neutrons/cm^2/s [10]. Previous measurements of the neutron flux in the Creighton mine quote 3.4 neutrons/cm^2/s in the 5400 ft level (norite) and 3.2 neutrons/cm^2/s in the 5600 ft level (red granite) [11]

The spectra resulting from the system of equations (5) are shown in figure 6. Some comments are in order:

- The differences between the background in the SNO cavity and the background at the 4600 ft level have implications on the final result of the gamma flux in the cavity. The assumption that the neutron flux and the Th contents (2614 keV gamma-ray flux) are correlated is arbitrary, although reasonable. We point out that the U contamination in the SNO bedrock and in shotcrete are roughly the same.

- The neutron flux has implication in the origin of the counts in the NaI detector. If events are produced inside the crystal by neutron activation or if arise from bombardment the crystal from outside, the shape of the detector's response will be affected.

- The gamma-ray flux in the SNO cavity, as obtained from our measurement and analysis, is summarized in table 5 below. These values correspond to the solution of the system of equations (5) for the spectrum γ_1. Errors associated to the flux are from quadrature sum of statistical errors combined with the estimated systematic errors (10%).

- The shape of the neutron spectrum in figure 6 presents a structure that we identify, at low energies with the decay of ^{128}I and ^{24}Na which are activated while the NaI is exposed to the neutron flux. The structure centered at around 6 MeV is identified with the prompt gamma-rays from neutron capture in I. We are currently studying these possibilities.

Table 5: Experimental gamma-ray fluxes at SNO cavity. These results correspond to the spectrum

γ_1 obtained from the solution of (5).

Energy interval (keV)	Flux ($h^{-1}cm^{-2}$)	Error (%)
0-1000	373.5586	10.0
1000-2000	710.5565	10.0
2000-3000	90.85286	10.0
3000-4000	1.972758	10.0
4000-5000	0.1038150E-01	11.6
5000-6000	0.2014590E-02	19.2
6000-7000	0.1279787E-02	18.6
7000-8000	0.2952307E-03	27.5
8000-9000	0.0000000E+00	0.0000000E+00

2.4 The effect in SNO of gamma flux above 3 MeV

A two step procedure was done in order to quantify the consequences of high energy gamma rays for the SNO experiment. In the first step we used GEANT 3.21 to track gamma-rays and its secondary particles from the wall of the cavity up to a spherical surface of 18 meters of diameter. The particle type, direction and position are then recorded and used as input for SNOMAN 2.09 [12], which track particles and generates Cerenkov photons in SNO. The GEANT simulation of the cavity uses the real cavity dimensions as measured in 15 different heights. Table 6 shows the radius of the cavity at a given height. The height values are relative and were adjusted so that the center of the cavity is at (0,0,0) [13].

Table 6: Height and Radius of the SNO Cavity.

Height (cm)	Radius (cm)	Height (cm)	Radius (cm)
1225.300	952.8000	-164.5901	1125.930
1146.050	968.3500	-249.9401	1133.550
822.9600	1049.730	-530.3501	1131.720
725.4199	1067.100	-719.3301	1088.440
527.3000	1090.880	-920.5001	1114.960
381.0000	1133.860	-1042.420	1100.630
115.8199	1137.820	-1225.300	1033.580
9.139893	1146.050		

The GEANT simulation generates the gamma-rays uniformly in the cavity walls in all directions in 1 MeV bins from 3 to 12 MeV. We studied two possible geometries: water filled cavity and air filled cavity. Table 7 shows the number of events generated in the cavity walls for each energy interval for the water fill geometry and for the air fill geometry.

Table 7: GEANT generated events

Energy interval (MeV)	Events generated H_2O	Events generated AIR
3 - 4	1.17×10^8	1.0×10^6
4 - 5	1.05×10^8	1.0×10^6
5 - 6	1.13×10^8	1.0×10^6
6 - 7	1.09×10^8	1.0×10^6
7 - 8	0.520×10^8	1.0×10^6
8 - 9	0.497×10^8	1.0×10^6
9 - 10	0.504×10^8	1.0×10^6
10 - 11	0.479×10^8	1.0×10^6
11 - 12	0.489×10^8	1.0×10^6

As a visual aid, figure 7 shows the projection of events generated in the cavity walls superimposed with the events which survive the water shield. Note the higher survival probability around the equator, where the passive water shielding is narrower

Figures 8 and 9 show the fraction of the gammas which arrive to the photomultiplier support structure (PSUP) level and give examples of the energy at which they will start to be tracked by SNOMAN. The plot on the left in figure 8 shows the fraction of gamma rays which arrive to the 9 meter radius sphere normalized to the number of gammas generated randomly in in the cavity walls. Full circles represent all gamma rays with energy above 1 MeV that arrive to the nine meter radius sphere. The triangles represent the non-degraded energies. On the right is plotted an example of the spectrum of the gamma rays at the nine meter level showing the degradation of energy. Similar plots are shown in figure 9 in the case of the air geometry.

Electrons or gamma-ray which reach the PSUP have their its position and momentum recorded at the end of the GEANT simulation. The information is then used as input for SNOMAN, the SNO dedicated Monte-Carlo, which tracks Cerenkov photons throughout the detector and simulates data as recorded by SNO. SNOMAN also provides tracking reconstruction and filtering.

For the purpose of this study, we set standard conditions to the filter and trigger of an event requiring that at least 10 photomultipliers fire and submitting the events to the standard event filter, the "time fitter" FTT.

The SNOMAN output is used to obtain the distribution of photomultipliers fired per gamma-ray generated in the cavity walls. This normalize probability density is then multiplied by the measured gamma-ray flux. The resulting distributions are shown in figures 10 and 11 for water fill geometry and for the air fill geometry respectively. Figures 10 and 11 show the expected NHITS distribution for 3 different selection conditions for the water filled detector and for the air geometry respectively:

- White spectrum: no condition imposed to the events i.e., all events which satisfy the trigger of 10 hits per event are recorded. For the water fill geometry 423.3 events per day will satisfy this condition while 7.35×10^7 events will satisfy this condition in the air fill geometry.

- Grey: the condition that the event was reconstructed in the D_2O volume, i.e., inside a 6 m radius sphere. 48.3 events per day will satisfy this condition in the water fill geometry and 1.38×10^7 will satisfy this condition for the air fill geometry.
- Hatched: the condition that the event was reconstructed inside a fiducial volume determined by a 5 m radius sphere. 9.7 events will survive this cut per day in the water fill geometry, while 6.31×10^6 events per day will satisfy this condition in the air fill geometry.

3 Comments and conclusions

We studied the gamma-ray background in the SNO cavity and evaluated the consequences of high energy gamma-rays for the SNO experiment.

The experimental value obtained for the flux of gamma-rays above 5 MeV in the cavity, is 0.086 ± 0.011 gammas/cm^2 per day. This value should be compared to previous estimations of the high energy gamma-ray background given by the "Blue Book", from MC calculations 0.08 gammas/cm^2 per day. More recent values are quoted by P. Skensved and B. C. Robertson on "Summary of Backgrounds in SNO". Their estimation of the flux of gamma-rays above 5 MeV in the SNO cavity is of 0.033 gammas/cm^2 per day.

The estimations given above for the number of events reconstructed and detected by SNO are to be regarded as a very conservative upper limit. On the simulation and data analysis side of the effects of this flux in SNO, we are using a very simple selection criteria. Optimization in the selection cuts and event reconstruction will further reduce the number of events which were wrongly reconstructed in the D_2O .

4 References

1. Sudbury Neutrino Observatory Proposal, SNO-87-12, October 1987.
2. A good reference for the Solar Models and updates is J. Bahcall's home page at *http://www.sns.ias.edu/ jnb/.*
3. A. A. Pomansky, NIM B 17, 406, 1986.
4. R. K. Heaton et. al., NIM A 364, 317, 1995.
5. GEANT 3.21, CERN Program Library, long writeup W5013
6. A. Smith and S. Flexser, "Radioactivities of rock samples from the SNO cavity excavation", LBL/LBF 10/10/93.
7. M. Chen, M.Sc. thesis, Laurentian University, 1995.
8. P. Jagam, private communication.

9. J.J. Thiessen, M.Sc. thesis, Queens University, 1992.

10. P. Belli et al., "Deep Underground Neutron Flux Measurement with Large BF_3 counters", Il Nouvo Cimento, 101A, 959, 1989.

11. SNO Collection of Annexes in Support of the main proposal. Annex-10, November 1987.

12. SNOMAN 2.09, Users Manual,

13. N. West, private communication.

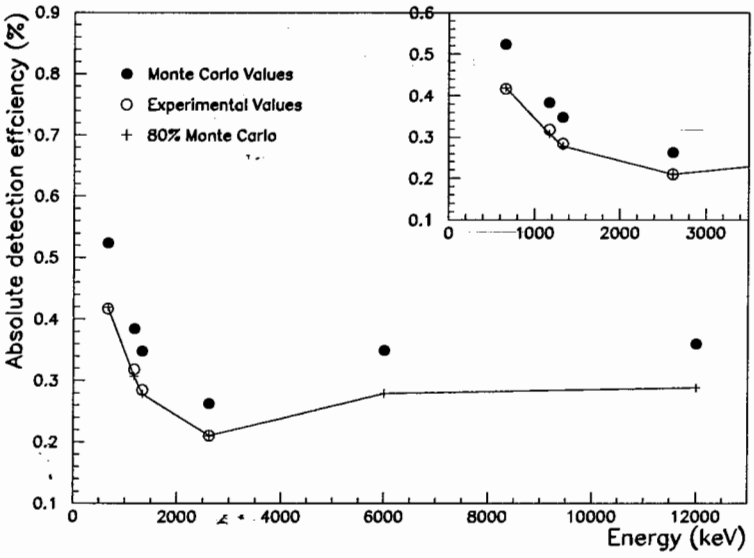

Figure 1: Absolute efficiency of the NaI detector at 19 inches. Point sources were used to obtain the experimental points. Values for the efficiency obtained by Monte Carlo calculations were also corrected for light collection effects.

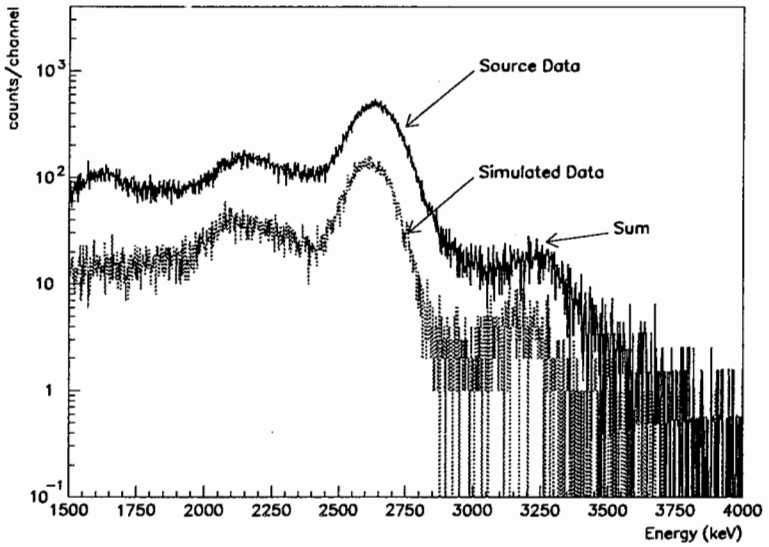

Figure 2: Quantitative comparison between the experimental response of the NaI crystal and the response calculated by Monte Carlo.

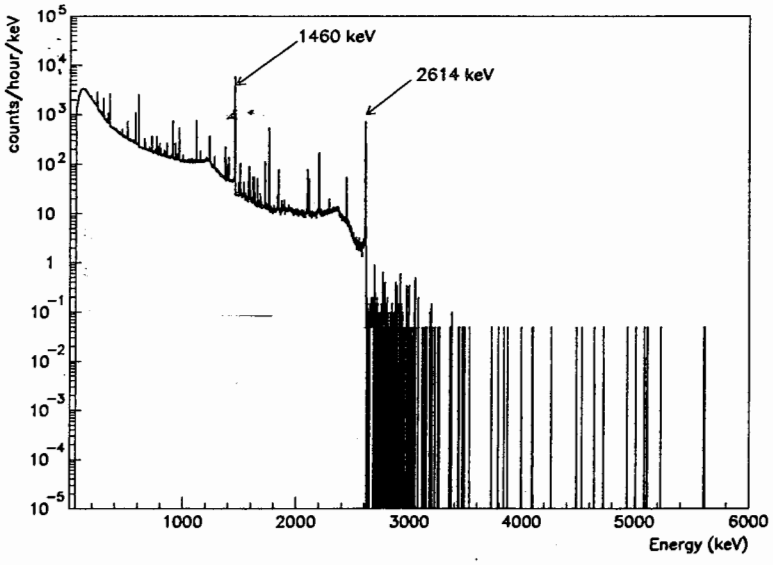

Figure 3: Spectrum SNOGE measured at the bottom of the SNO cavity before the lining with shotcrete. Data was accumulated for 20.65 h.

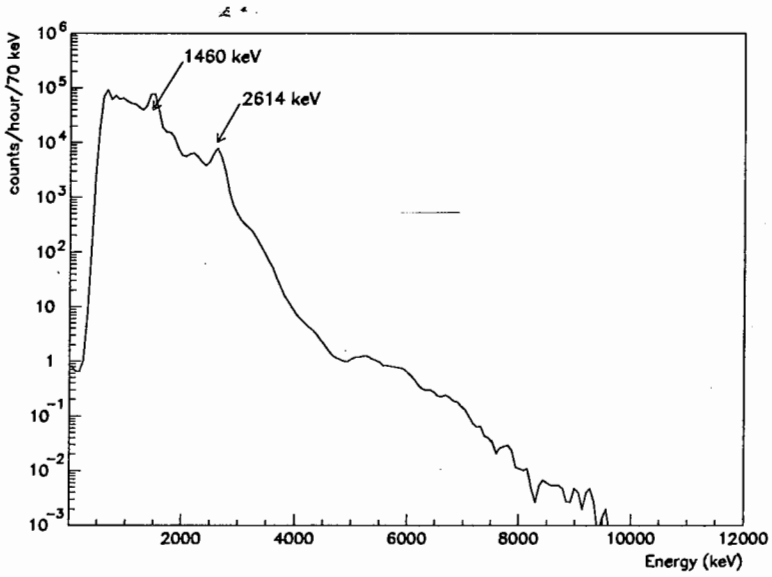

Figure 4: Raw data from recent measurement of gamma flux in the SNO cavity using a NaI detector. Data was accumulated for 1490.41 hours. Channel width = 70 keV.

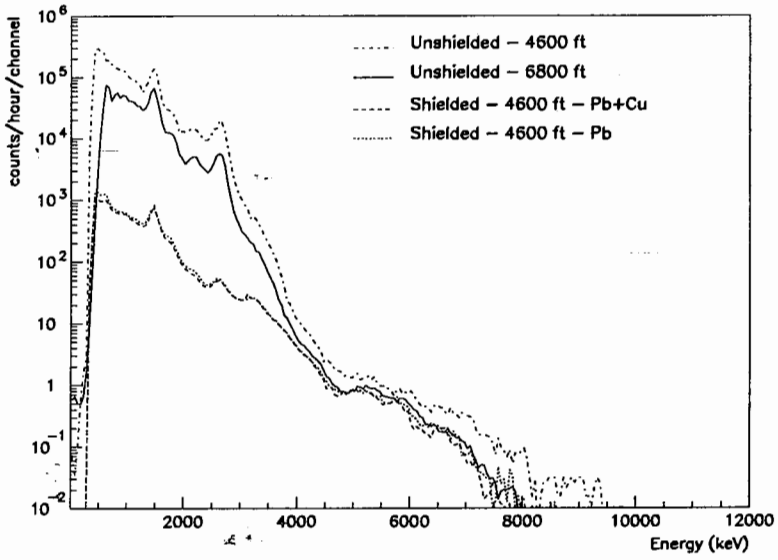

Figure 5: Comparison between the data available. Data was obtained in 4 different conditions: Unshielded inside the SNO cavity at the 6800 ft level; unshielded at the 4600 ft level and with 2 different shielding at the 4600 ft level. Channel width = 50 keV.

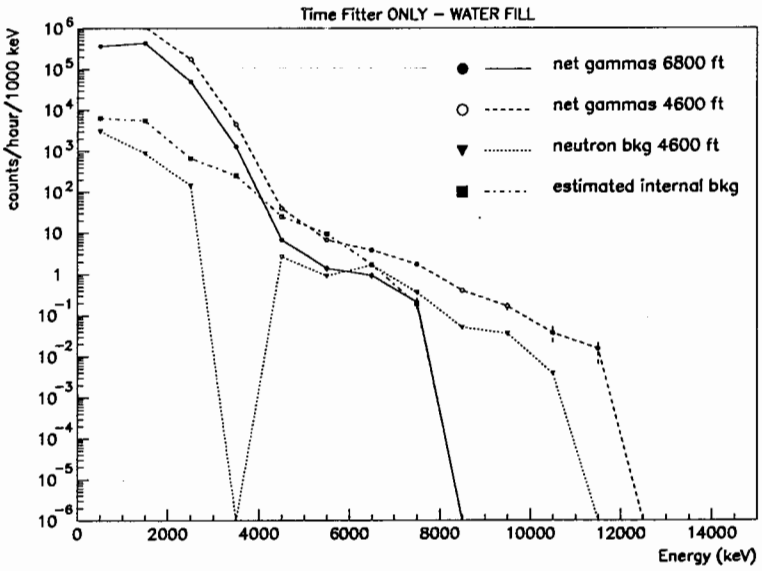

Figure 6: Spectra solution of the system of equations (5).

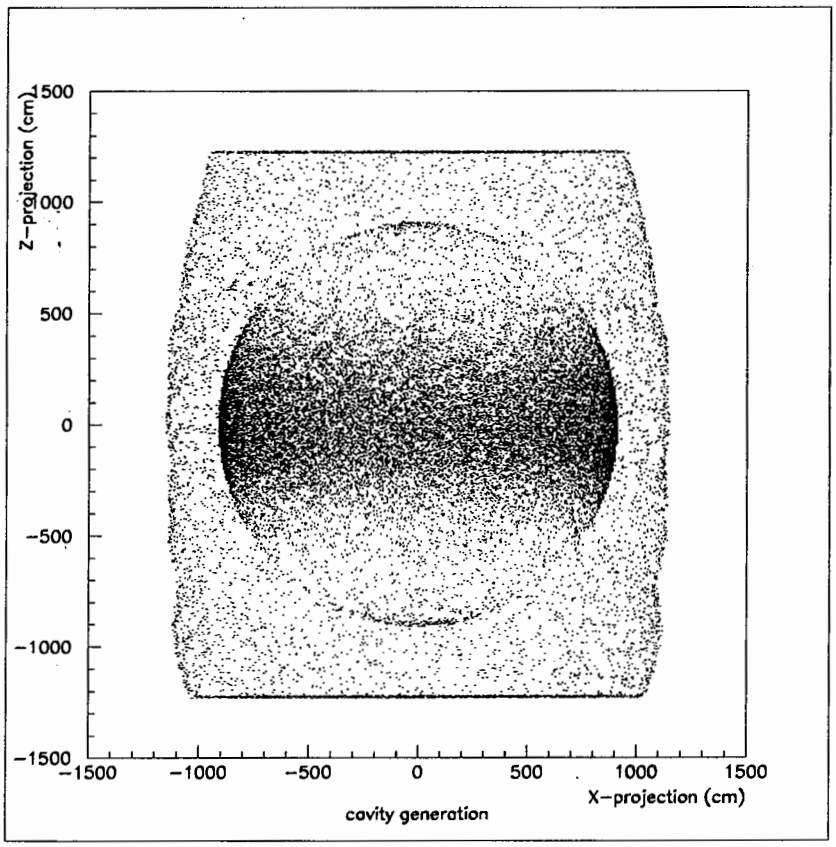

Figure 7: Projection of the GEANT generation in a water filled geometry. In this plot are represented the XZ projection of the position at which events are generated in the cavity walls superimposed to the position where particles intercept a 9 meter sphere. From this sphere on particles are tracked by SNOMAN.

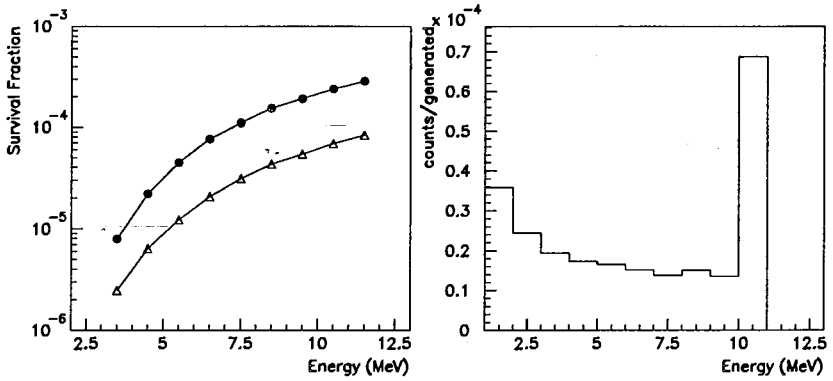

Figure 8: Water Geometry. LEFT: Fraction of particles which arrive to the 9 m surface from which particles are treated by SNOMAN. The full circles represent the number of gammas of any energy that arrive to the PSUP once a gamma of energy E gas generated in the cavity walls. Triangles represent the number of gammas of energy E which arrive to the PSUP once gammas of the same energy were generated in the cavity walls. RIGHT: Energy spectrum of the gammas which arrive to the 9 m surface. In this case gammas with energies between 10 and 11 MeV were generated at the cavity walls.

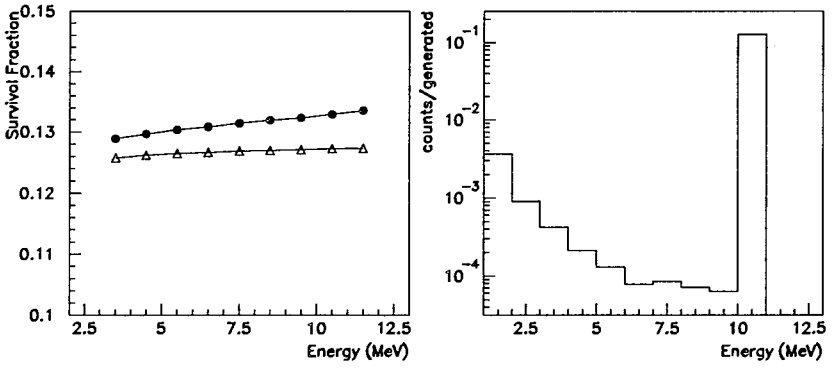

Figure 9: Air Geometry. LEFT: Fraction of particles which arrive to the 9 m surface from which particles are treated by SNOMAN. RIGHT: Energy spectrum of the gammas which arrive to the 9 m surface. In this case gammas with energies between 10 and 11 MeV were generated at the cavity walls.

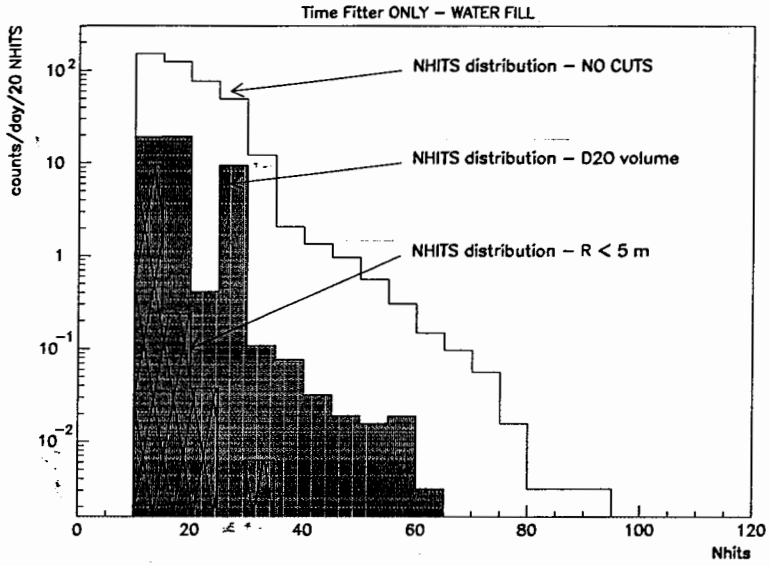

Figure 10: Water filled NHITS distribution in SNO obtained from the measured gamma flux in the cavity with a NaI detector for the 3 selection conditions specified in the text.

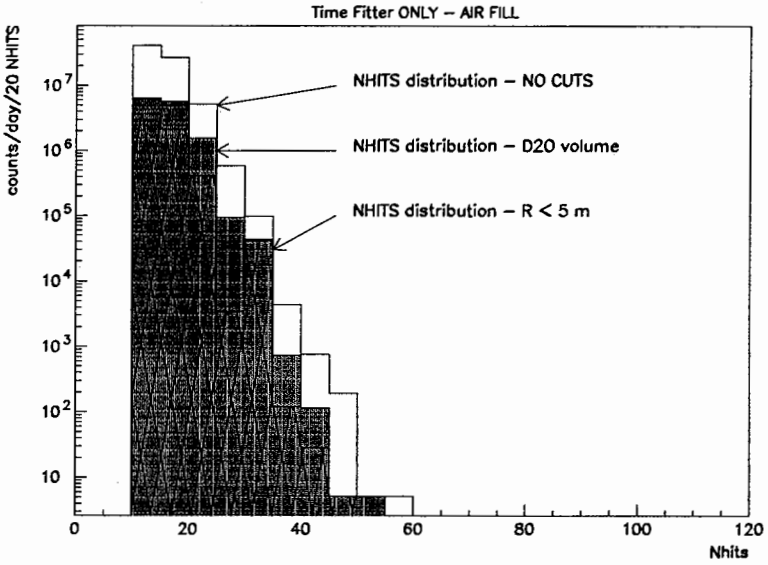

Figure 11: Air filled NHITS distribution in SNO obtained from the measured gamma flux in the cavity with a NaI detector for the 3 selection conditions specified in the text.